iScience, Volume *23*

Supplemental Information

Complete Photocatalytic Mineralization of Microplastic on TiO_2 Nanoparticle Film

Iqra Nabi, Aziz-Ur-Rahim Bacha, Kejian Li, Hanyun Cheng, Tao Wang, Yangyang Liu, Saira Ajmal, Yang Yang, Yiqing Feng, and Liwu Zhang

Supplemental Information for

Complete Photocatalytic Mineralization of Microplastic on TiO_2 Nanoparticle Film

Iqra Nabi[1], Aziz-Ur-Rahim Bacha[1], Kejian Li[1], Hanyun Cheng[1], Tao Wang[1], Yangyang Liu[1], Saira Ajmal[1], Yang Yang[1], Yiqing Feng[1], and Liwu Zhang[1, 2]*

[1]Shanghai Key Laboratory of Atmospheric Particle Pollution and Prevention, Department of Environmental Science & Engineering, Fudan University, Shanghai, 200433, Peoples' Republic of China

[2]Shanghai Institute of Pollution Control and Ecological Security, Shanghai, 200092, Peoples' Republic of China

*Corresponding Author:

E-mail: zhanglw@fudan.edu.cn ; Phone/Fax: +86-21-6564-2781

Table of contents:

Supplementary Figures 1 to 18
Supplementary Tables 1 to 2
Transparent Methods
Supplemental References

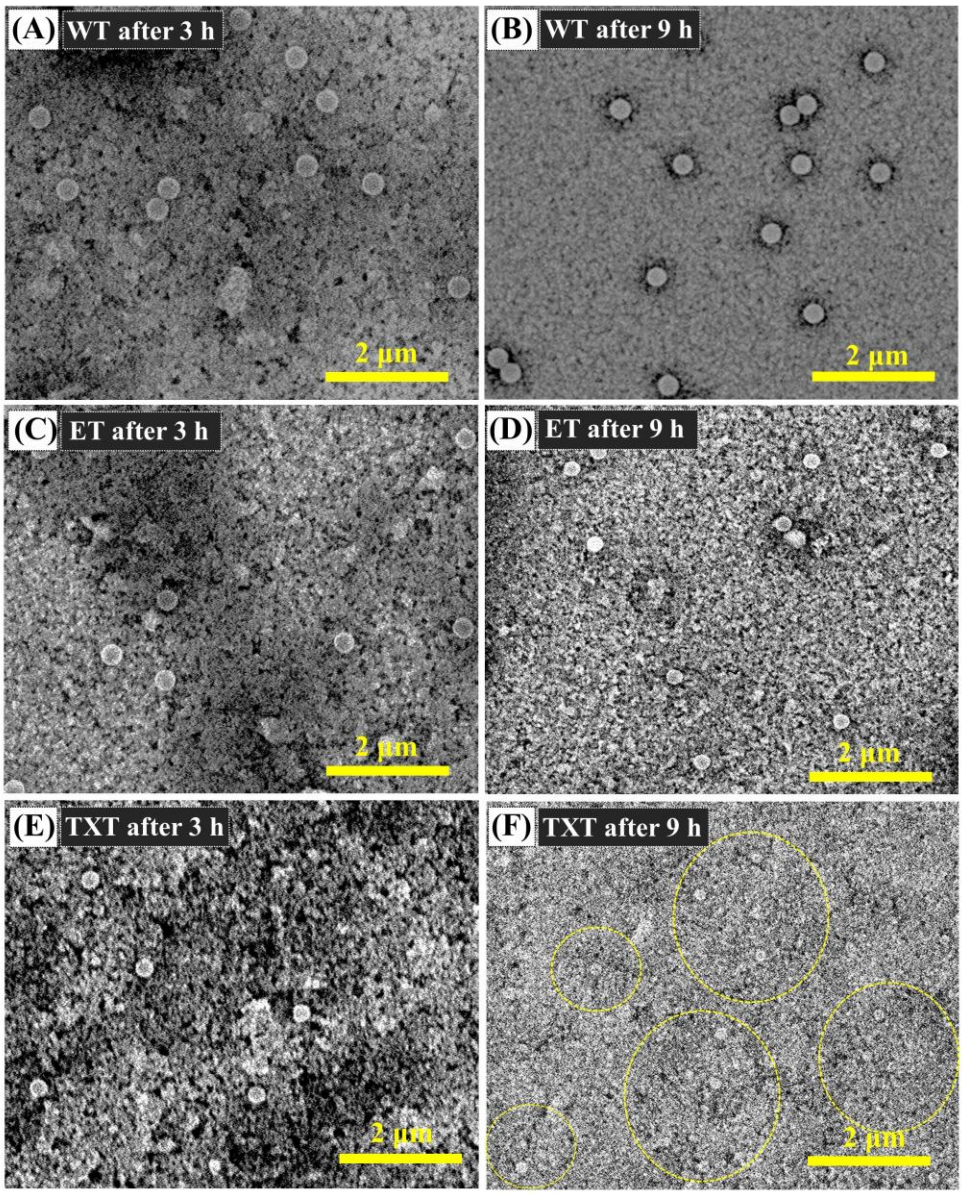

Figure S1. SEM images of 400 nm PS on TiO_2 based catalysts under 365 nm UV light. Related to Figure 1. (A, B) WT after 3 and 9 h irradiation **(C, D)** ET after 3 and 9 h irradiation and **(E, F)** TXT after 3 and 9 h irradiation. (SEM images were taken through phenom Prox).

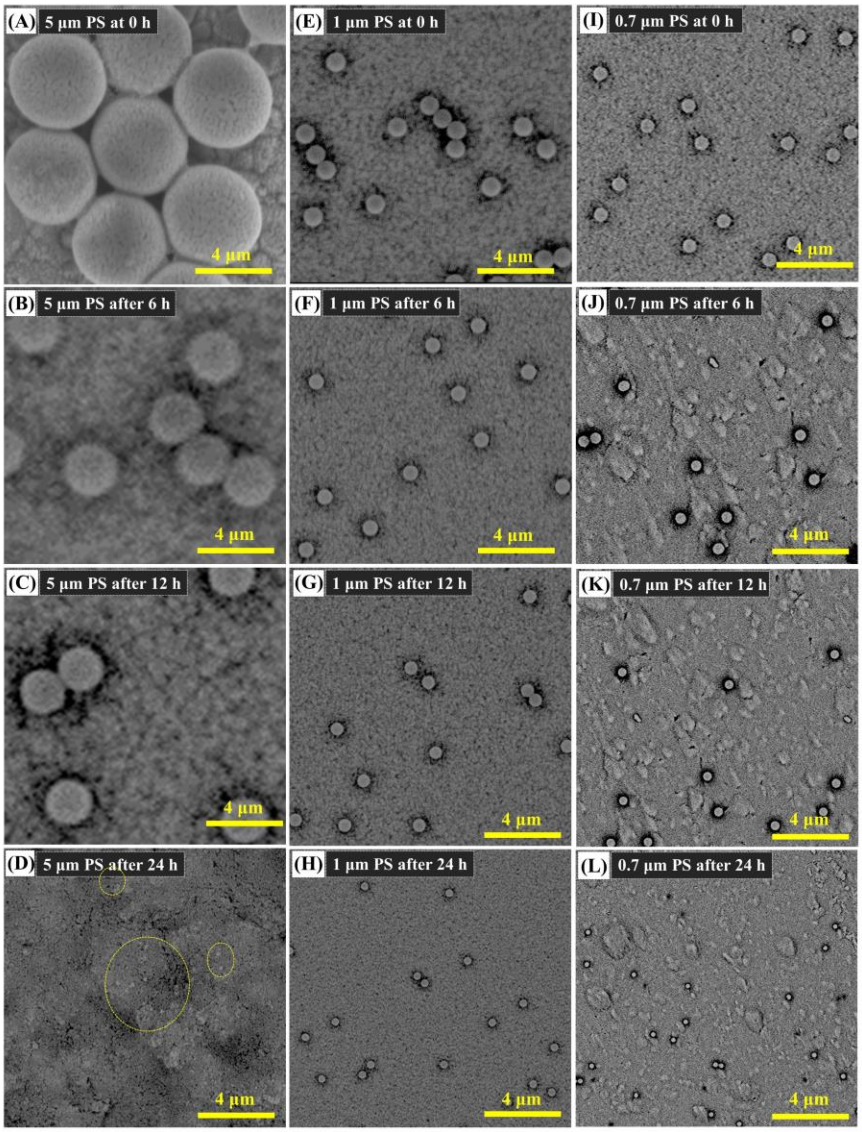

Figure S2. SEM images of 5 µm, 1 µm and 700 nm PS on TXT film. Related to Figure 2. (A) 5 µm PS at 0 h of UV irradiation **(B)** 5 µm PS at 6 h of UV irradiation **(C)** 5 µm PS at 12 h of UV irradiation **(D)** 5 µm PS at 24 h of UV irradiation **(E)** 1 µm at 0 h of UV irradiation **(F)** 1 µm at 6 h of UV irradiation **(G)** 1 µm at 12 h of UV irradiation **(H)** 1 µm at 12 h of UV irradiation **(I)** 700 nm PS at 0 h of UV irradiation **(J)** 700 nm PS at 6 h of UV irradiation **(K)** 700 nm PS at 12 h of UV irradiation **(L)** 700 nm PS at 24 h of UV irradiation. (SEM images were taken through phenom Prox and 5 µm PS degradation experiment was carried out through 254 nm UV light while other experiments (1 µm and 700 nm**)** was done under 365 nm UV light).

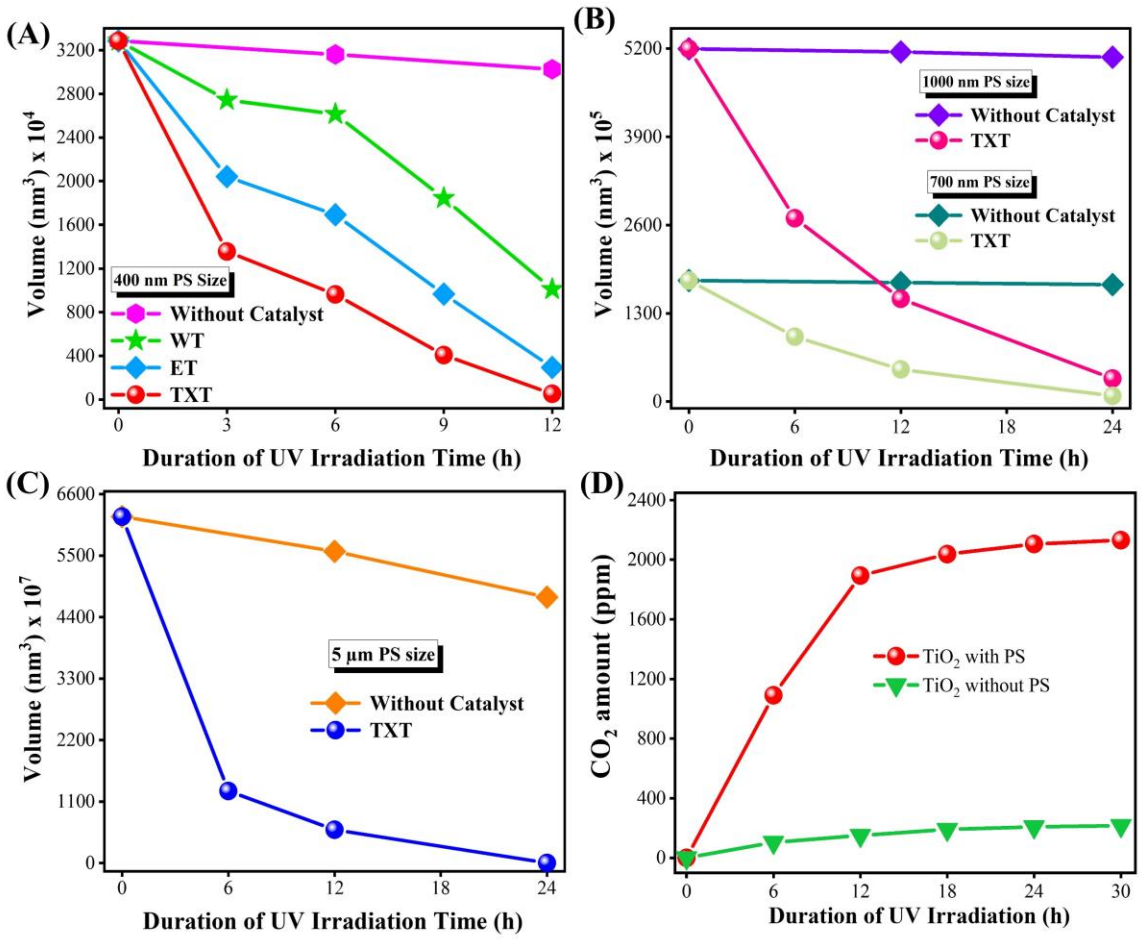

Figure S3. Volume changes of varying size PS and CO_2 concentration. Related to Figure 2. (A) 400 nm PS on WT, ET, and TXT film under 365 nm UV light. **(B)** Volume change of 1 µm and 700 nm PS by TXT film under 365 nm UV light. **(C)** 5 µm PS volume change by TXT film under 254 nm UV light. **(D)** CO_2 concentrations in TiO_2 with and without PS at different stages of photodegradation reaction.

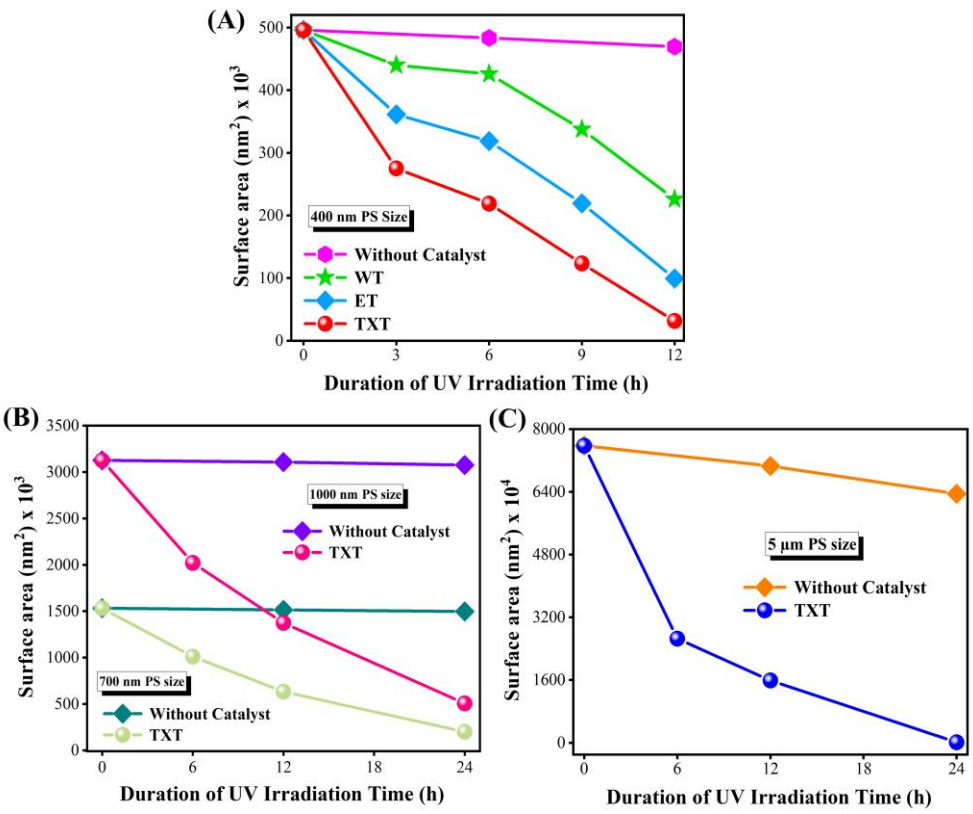

Figure S4. Surface area changes in varying size PS. Related to Figure 2. (A) 400 nm PS on WT, ET, and TXT film under 365 nm UV light. **(B)** Surface area change of 1 µm and 700 nm PS by TXT film under 365 nm UV light. **(C)** 5 µm PS surface area change by TXT film under 254 nm UV light. (Figure S4A-C displays the prominent changes in surface area of varying sizes of PS against different times under UV light irradiation. Surface area changes in 400 nm PS on FTO (without photocatalysts) were negligible, while an effective change was observed on TXT, ET, and WT films (Figure S4A). Additionally, by comparing the surface area changes of PS on fabricated films, TXT showed higher performance, which was due to its unique properties such as bandgap, crystal shape, charge separation, etc. Figure S4B suggests that the surface area in 700 nm PS and 1 µm PS were also changed with the increase in irradiation time. Moreover, a significant change in surface area was observed in 5 µm PS (Figure S4C). Notably, the surface area of varying sizes of PS was decreased with the increase in irradiation time).

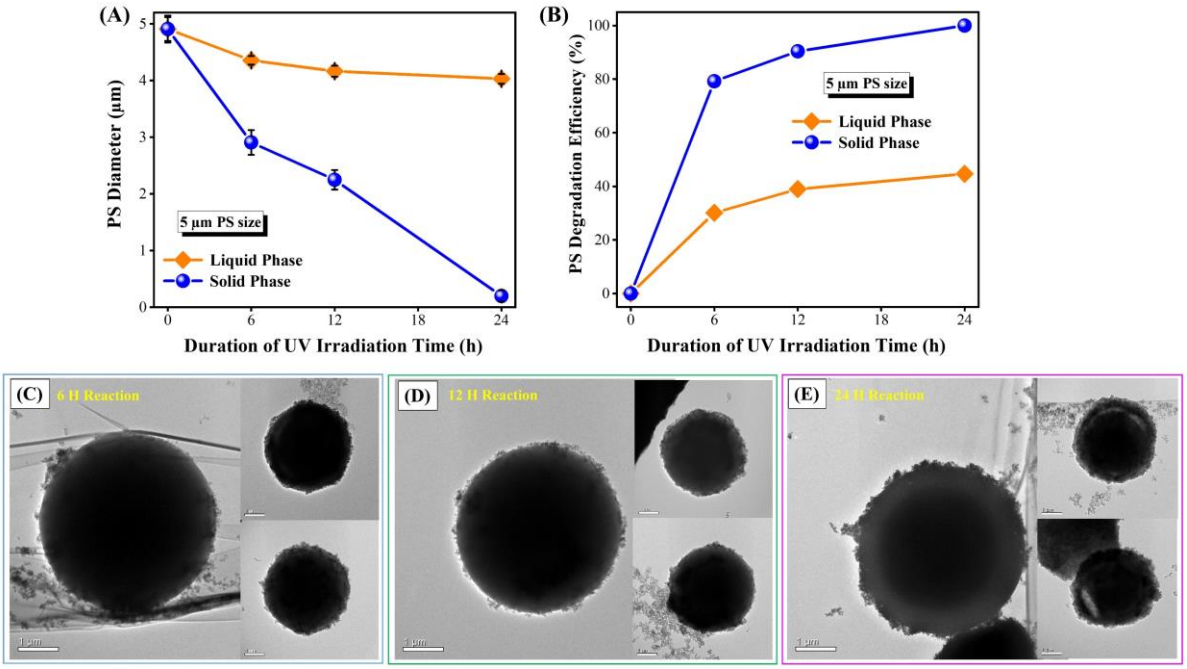

Figure S5. Solid-phase vs. liquid-phase degradation of 5 μm PS under 254 nm UV light with different irradiation time interval. Related to Figure 2. (A) Diameter change of 5 μm PS **(B)** Degradation efficiency (%) of 5 μm PS **(C)** TEM images of 5 μm PS spheres in liquid phase after 6 h reaction. **(D)** TEM images of 5 μm PS spheres in the liquid phase after 12 h reaction. **(E)** TEM images of 5 μm PS spheres in the liquid phase after 24 h reaction. The experiment was carried out at its natural pH.

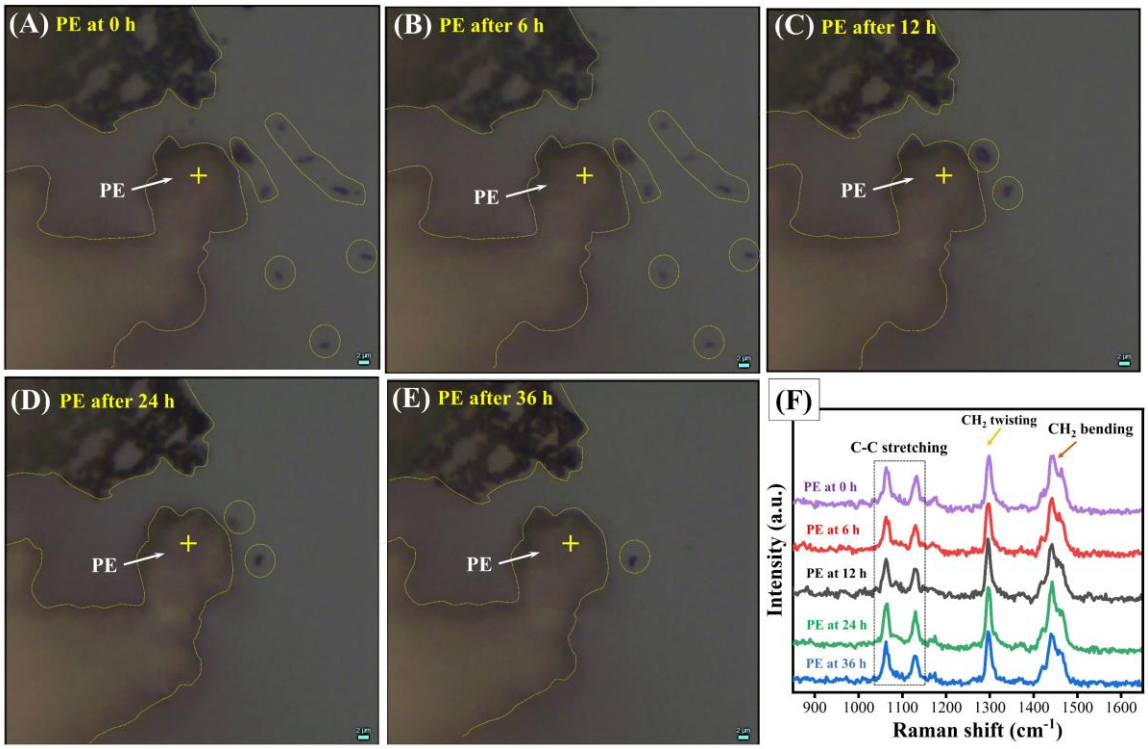

Figure S6. Photocatalytic degradation of PE on FTO (without catalyst) under 254 nm UV light. Related to Figure 3. (A) PE at 0 h **(B)** PE after 6 h **(C)** PE after 12 h **(D)** PE after 24 h **(E)** PE after 36 h **(F)** RAMAN spectrum of PE with different time profiles. (Highlighted parts present PE, and the same point was used for Raman imaging and detection throughout the experiment).

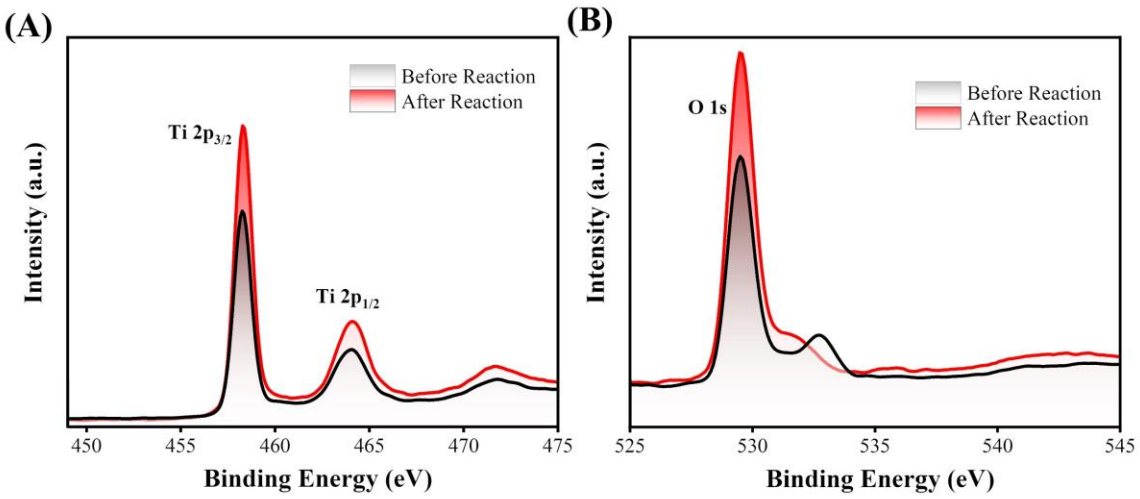

Figure S7. X-ray photoelectron spectra of TXT film before and after the reaction. Related to Figure 2-3. (A) Ti 2p **(B)** O1s. (X-ray photoelectron spectroscopy (XPS) analysis was performed to determine the oxidation state of TiO_2 film before and after the degradation experiment. Figure S7A displays the spectra of Ti 2p, in which two peaks were detected at 458.38 and 464.08 eV, corresponding to the binding energy of Ti $2p_{3/2}$ and Ti $2p_{1/2}$ due to the presence of Ti $^{4+}$ state. Figure S7B presents the spectra of O 1s spectra, in which binding energy of the O 1s was observed at 532.18 eV due to the presence O^{2-} in TiO_2 lattice. After reaction, the increase in binding energy was due to the oxidation of PS particles).

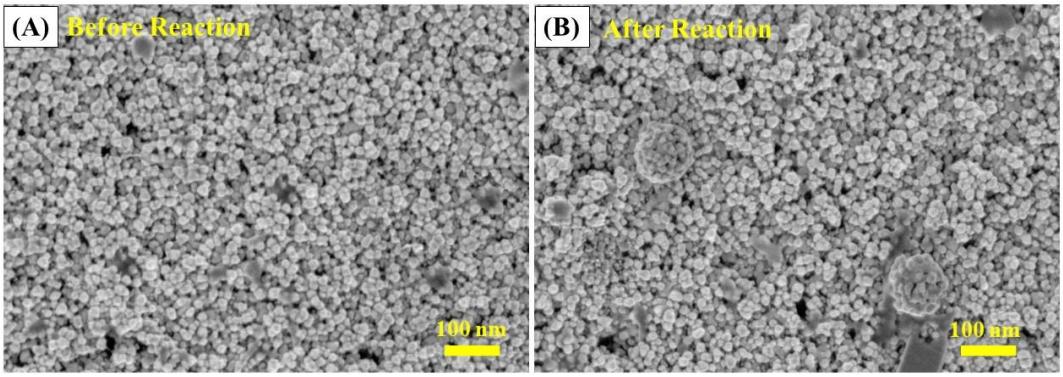

Figure S8. Morphological analysis of TiO_2 films (TXT)) before and after 12 h reaction. Related to Figure 2-3.

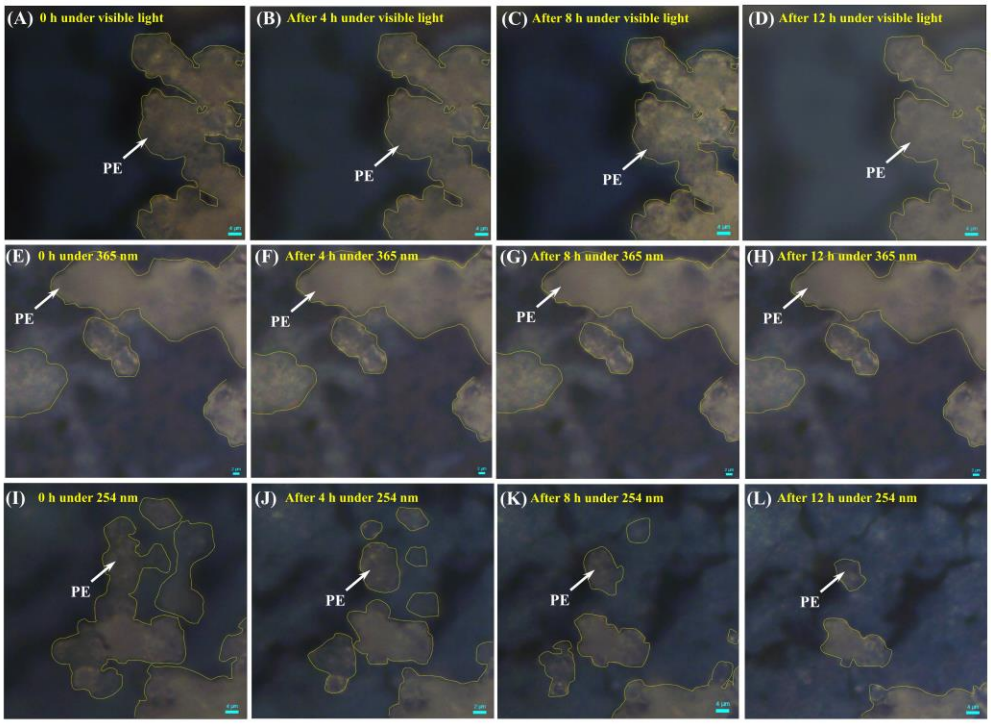

Figure S9. Photocatalytic degradation of PE on TiO_2 film under different irradiation sources. Related to Figure 3. (A-D) PE degradation under visible light **(E-H)** PE degradation under 365 nm UV light **(I-L)** PE degradation under 254 nm UV light. (Highlighted parts present PE). Photodegradation of microplastic depends on various parameters such as the size of microplastic, concentration of microplastic quantity, catalyst amount, light intensity, irradiation time, surface area, and light absorbance of catalyst. Figure S9 shows the degradation of PE under different light sources. It can be seen that the PE degradation was insignificant under visible and 365 nm UV light. A significant change in PE degradation was observed under 254 nm UV light due to its short wavelength and strong energy, which leads to the fast generation of free radicals in the plastic matrix, preferring radical's combination comparative to reaction with oxygen (Shyichuk and White, 2000). The UV light has a particular impact on the degradation of polymers, especially in the range from 290-400 nm, while the influence of visible light was negligible (Decker and Mayo, 1973). The outcomes of this result suggested that 254 nm UV light is more powerful for the degradation of microplastics.

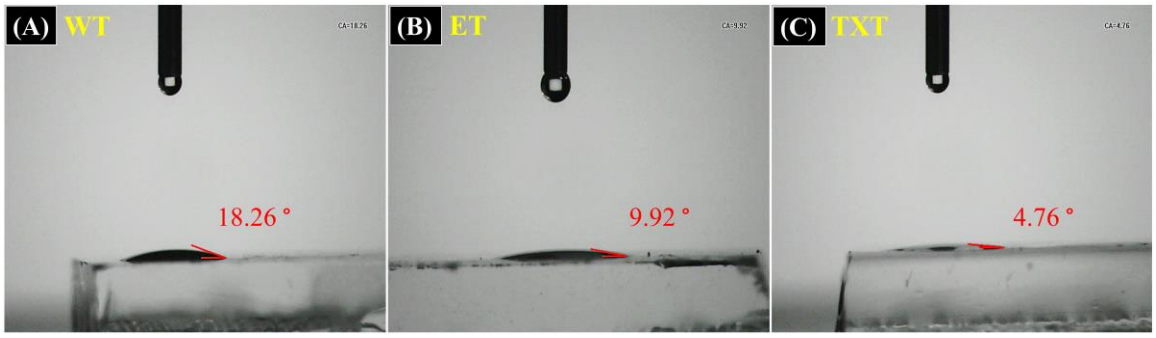

Figure S10. Hydrophilicity Measurement. Related to Figure 4. The water contact angle of **(A) WT, (B) ET, and (C) TXT (Sessile water drops on fabricated films).** Water contact angle measurement is the most common method for determining the surface hydrophilicity changes in films (WT, ET, and TXT), as presented in Figure S10. Basically, the wettability of a material is directly proportional to the surface tension of the liquid and inversely proportional to the contact angle and pore size of the material. The application of a surfactant not only reduces the surface tension of liquid but also causes a decrease in contact angle. It has been observed that the ET and WT films have a contact angle of 9.92° and 18.26°, which were higher as compared to that of TXT. The smaller contact angle value (4.76°) of TXT representing that the Triton X-100 not only improves the wettability but also smooth the film.

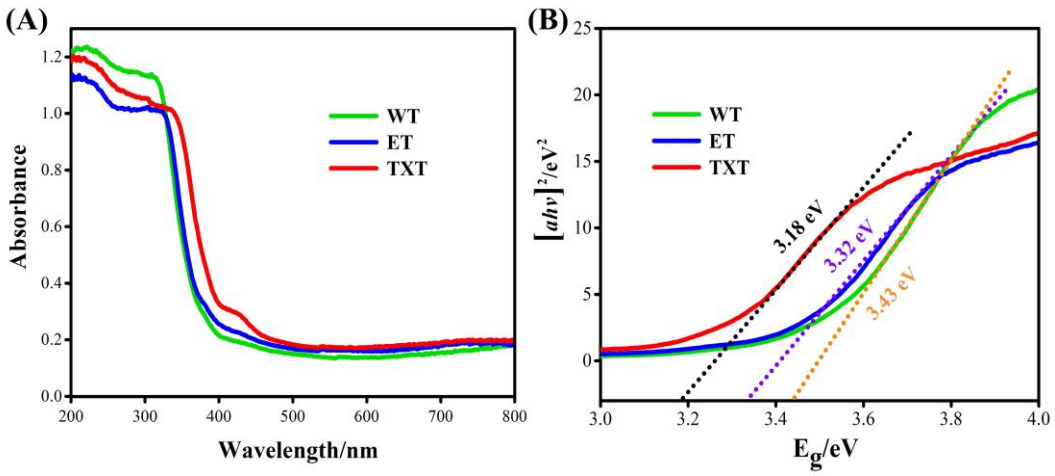

Figure S11. Optical Measurements. Related to Figure 4. (A) UV–vis absorption spectrum of TXT, ET, and WT **(B)** The Tauc plot of the TXT, ET, and WT nanoporous film. (UV–vis diffraction reflection spectroscopy (UV–vis DRS shows the absorption edges at about 390 nm representing the strong UV absorption region of WT and ET, while in TXT, a noticeable shift in the absorption edge towards the visible region at wavelength > 400 nm was observed (Figure S11A). The shift in the visible region has been claimed as a consequence of exciton confinement with a decrease in particle size indicative of the quantum size effect (Satoh et al., 2008). The bandgap of a semiconductor photocatalyst is linked with its absorption wavelength, and the bandgap decreases with an increasing absorption edge (Karthiga et al., 2015). The bandgap value of TXT, ET, and WT catalysts are 3.18, 3.32, and 3.43 eV, respectively (Figure S11B). The result confirms that triton X-100 based TiO_2 can efficiently improve the light absorption).

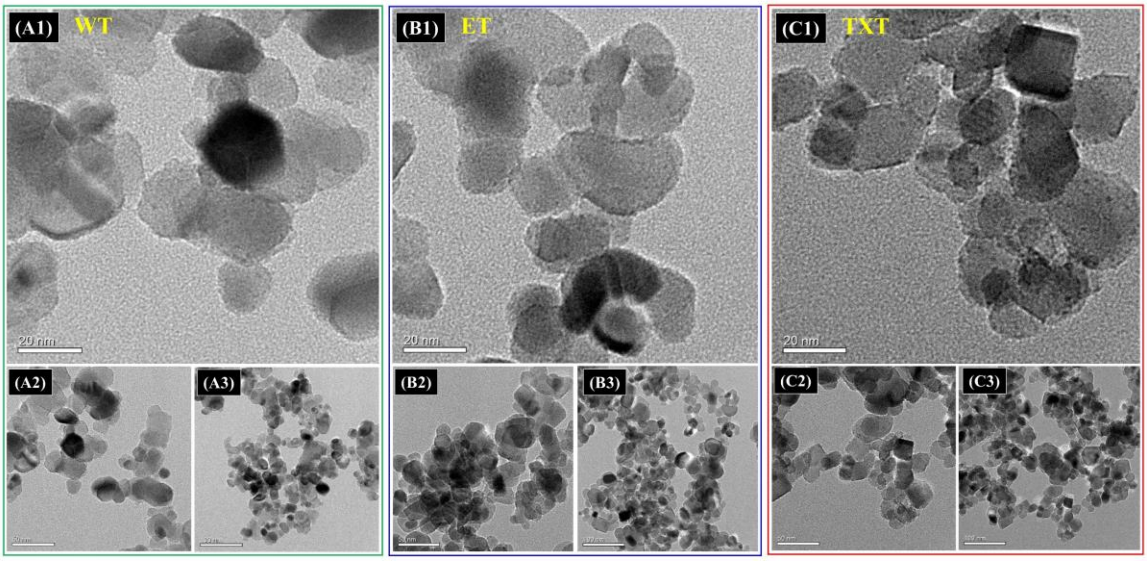

Figure S12. TEM images of TiO_2 films with 20 nm, 50 nm, and 100 nm scale bars. Related to Figure 4. (A1-A3) WT film. **(B1-B3)** ET film. **(C1-C3)** TXT film.

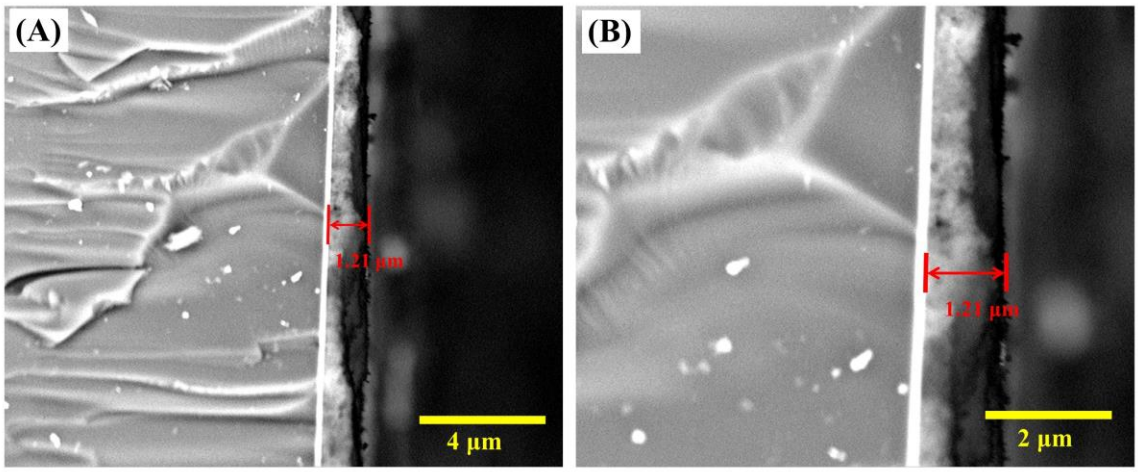

Figure S13. The cross-sectional SEM images of TiO_2 nanoparticles film. Related to Figure 4.

(A) TXT film at 4 µm scale bars. **(B)** TXT film at 2 µm scale bars.

Table S1. BET surface area, pore-volume, and pore size of the prepared catalysts. Related to Figure 4, S14.

Sample	BET surface area (m^2/g)	Pore volume (cm^3/g)	Pore size (nm)
WT	50.65	0.329	21.50
ET	53.13	0.357	21.19
TXT	55.74	0.390	34.69

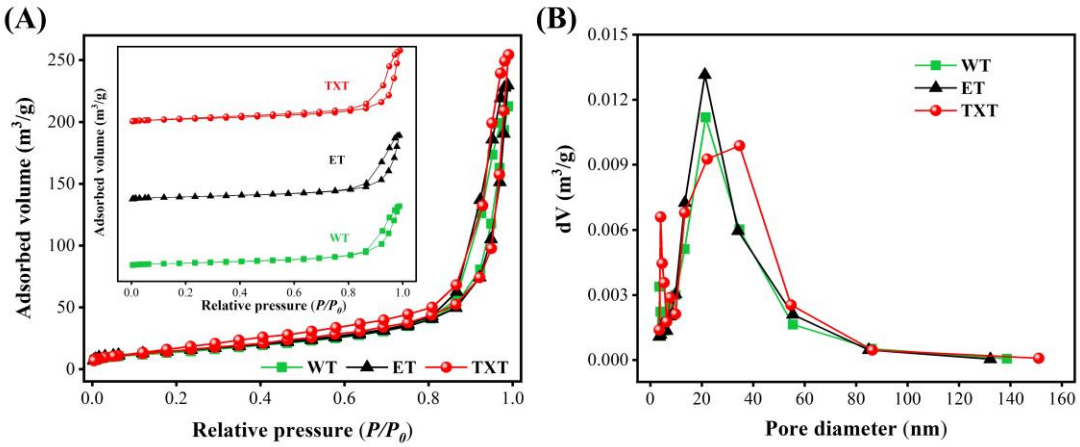

Figure S14. Nitrogen isotherm and pore diameter distribution of TiO_2 films. Related to Figure 4. (A) Nitrogen isotherm of TXT, ET, and WT **(B)** Pore diameter distribution curve of TXT, ET, and WT. (Specific surface area and pore-size distribution analysis of prepared TiO_2 films were measured through Brunauer-Emmett-Teller (BET). Table S1 shows the BET results of TXT, ET, and WT films which were calculated by using the multipoint BET method. It was interesting to observe that TXT film has a high surface area, pore-volume, and pore size as compared to ET and WT films. It can be seen in Figure S14A, all TiO_2 films show the type H3 accordance with BDDT classification presenting the existence of mesopores. Figure S14B shows that the pore diameter of TXT film was higher as compared to the ET and WT films).

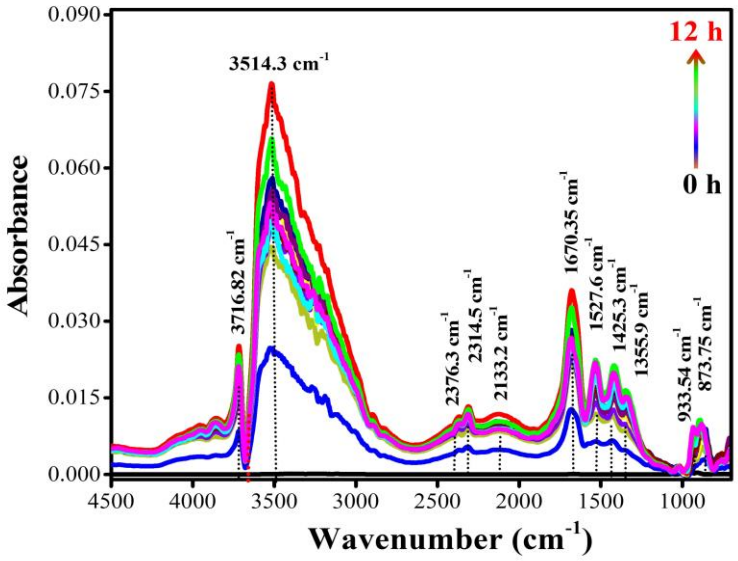

Figure S15. *In-situ* DRIFTs spectrum of PS with a time interval. Related to Figure 5.

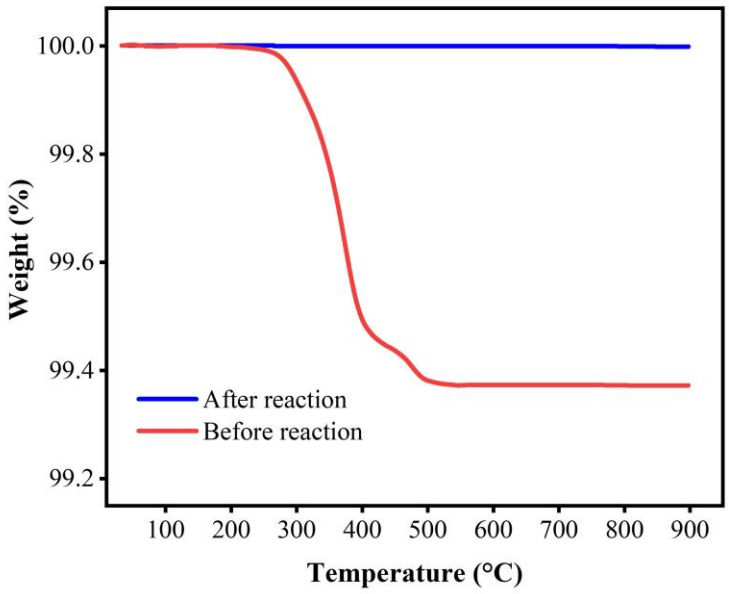

Figure S16. Mineralization of PS. Related to Figure 2. Thermogravimetric analysis of polystyrene loaded TiO_2 film before and after UV irradiation. (The complete mineralization was examined through thermogravimetric analysis (TGA), and the curves are presented in Figure S16. TGA of polystyrene (PS) loaded TiO_2 film showed different weight loss percentages at different temperatures before and after UV irradiation. Before reaction, thermal decomposition of polystyrene began at 263 °C, and a sudden decrease in weight was noticed at a narrow temperature range from 234-274 °C accompanied with a shoulder peak at about 280 °C. The complete decomposition of PS was taken place at 490 °C and then directly changed to gaseous species. Interestingly, negligible change in the TGA curve was observed after the degradation reaction, signifying the complete mineralization of PS and stability of the TiO_2 sample).

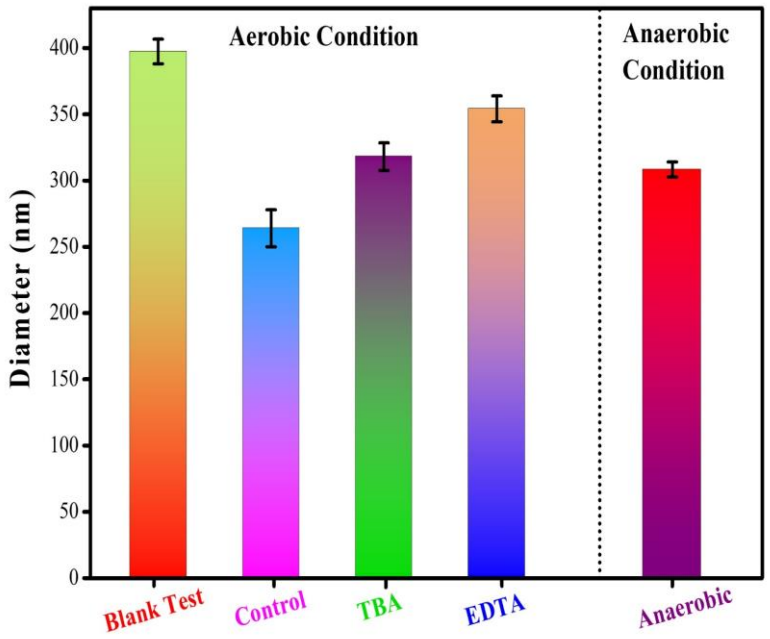

Figure S17. Detection of active species. Related to Figure 5. Hole Scavenging experiment result after 6 h of photoirradiation (Blank test was conducted without a photocatalyst (PS was dropped on cleaned FTO) control experiment was done on TXT film, 10 mM EDTA and 1000 mM TBA was added in 2 mL PS solution and 30 µL PS was dropped on TXT film for active species detection).

Table S2. Microplastics degradation reported by various studies. Related to Figure 2.

Catalysts	Morphology	Microplastics Type	Degradation System	Degradation Efficiency	Light Source	Reference
PE/N-TiO_2	Powder	HDPE	Liquid	6.40 % after 20 h	Fluorescent visible light	(Ariza-Tarazona et al., 2019)
C, N-TiO_2	Powder	HDPE	Liquid	71.77 % after 50 h	LED lamp with visible spectrum	(Ariza-Tarazona et al., 2020)
Mn@NCNTs	Powder	PE	Liquid	54 % after 8 h	0.2 g/L; PMS at 160℃	(Kang et al., 2019)
Photooxid-ation	-	^{14}C-PS	Liquid	28.1 % after 48 h	254 nm UV light	(Tian et al., 2019)
TiO_2	Film	PS	Solid	99.99 % after 24 h	254 nm UV light	This study
TiO_2	Powder	PS	Liquid	44.66 % after 12 h	254 nm UV light	This study

Here, HDPE = High-density polyethylene; PE = Polyethylene; ^{14}C-PS = Adioactively polystyrene, PS = Polystyrene.

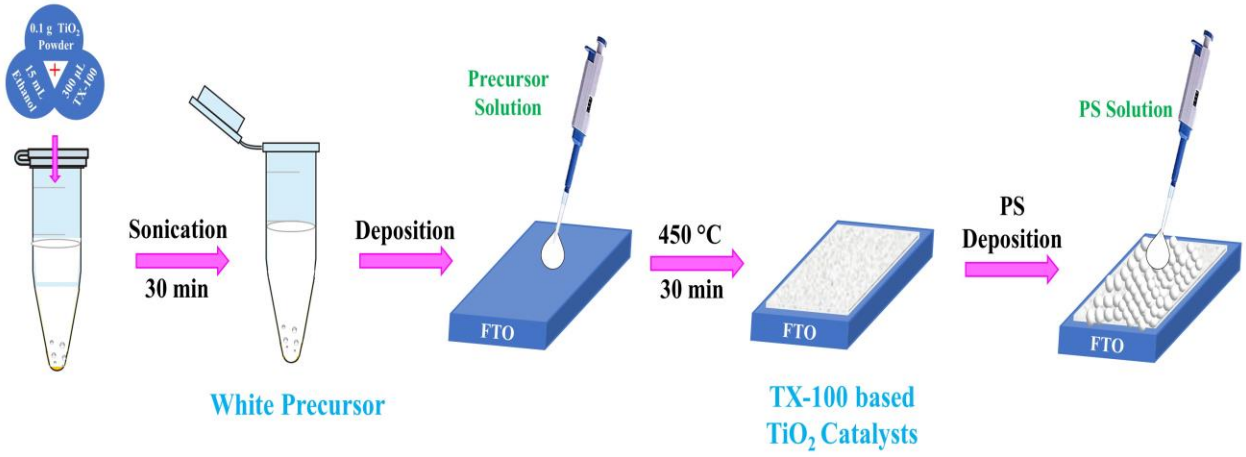

Figure S18. Schematic illustration of photocatalyst fabrication. Related to Figure 4. (At the initial stage, the TiO_2 powder was ground, after getting fine powder ethanol, and Triton X-100 was added to make a precursor solution. This precursor solution was dropped on FTO following the calcination process. A number of the coating can be increased to attain the desired film thickness).

Transparent Methods

Material Growth

Precursor solution of TiO_2 was prepared by grinding the TiO_2 (P25) powder (80 % anatase, and 20 % rutile from Degussa, Germany) in a mortar. The stuck TiO_2 powder inside mortar was removed with a spatula in order to grind aggregates. After getting the fine powder, 1 mL of DI water and 300 μL of Triton X-100 (Sinopharm Chemical Reagent Co., Ltd. China) were added dropwise and ground to make a paste. Triton X-100 was used as a non-ionic surfactant. Furthermore, 15 mL of ethanol (China General Reagent Co., Ltd.) was added dropwise into TiO_2 paste. The obtained precursor solution was sonicated 30 min, stirred for 40 min, and then named as TXT based TiO_2. Ethanol-based TiO_2 (ET) photocatalyst was synthesized by the same method except Triton X-100. Water-based TiO_2 (WT) was prepared by adding only DI water in TiO_2 powder.

Microplastics PS and PE were studied as a model pollutant. They were chosen based on their morphology, environmental abundance, and global production. PS spheres had a smooth surface and a definite size. Different sizes of PS spheres were studied due to their specific size while polyethylene had a rough texture and irregular shaped different sized particles. Microplastics solutions of PS and PE were prepared by the following method. 20 μL of standard concentrated solution of PS spheres (Standard polystyrene microspheres from Huge) were added in 20 mL of DI water and sonicated for 30 min. PE solution was prepared by adding 0.005 g of commercial PE powder (PE-50200 from Shanghai Youngling Electromechanical Technology Co., Ltd. China) in 5 mL of DI water and sonicated for 30 min.

Film Fabrication

The nanoporous WT, ET, and TXT based TiO_2 structures were fabricated on piranha [H_2SO_4: H_2O_2 = 3:1] cleaned FTO glasses (Wuhan Jinge-Solar Energy Technology Co., Ltd. China). The precursor solution of TiO_2 (25 μL) was dropped on conduction side of FTO (covered area 1.25 × 1 cm^2) dried in airflow oven at 70 ℃ and calcined at 450 ℃ for 30 min with a ramping rate of 5 ℃ min^{-1}. The schematic illustration is given in Figure S18.

Characterization

To study the crystal structure of synthesized TXT, ET, and WT based TiO_2 photocatalysts, X-ray diffraction (XRD) analysis was done. XRD spectra were collected by Bruker D8 Advance (XRD) with a Cu Kα radiation value (λ=1.54 Å) ranging from 10° to 70° (2θ) with a scanning speed of 2° min^{-1}. Raman spectrum and imaging were recorded by using the Raman xploRA plus spectrometer (HORIBA), with a green laser (λ = 532 nm) as an excitation source and Raman microscope objective 50x. The morphological characteristics of synthesized catalyst (TXT, ET, WT) and PS spheres were analyzed through field emission scanning electron microscopy (FE-SEM), transmission electron microscope (TEM), and phenom Prox. Each sample was sputtered with gold before SEM analysis. The size of PS spheres was calculated using ImageJ software. To examine the light absorption and optical band gap of fabricated photocatalyst films, the UV–vis absorption spectra were acquired by using a UV–vis diffraction reflection spectroscopy (SHIMADZU UV–2600). Specific surface area and pore-size distribution analysis of prepared TiO_2 films were measured through Brunauer-Emmett-Teller (BET). Amperometric *i-t* curve measurement was performed on an electrochemical station (CHI 660E, Shanghai Chenhua Co., Ltd. China) with a 300 W Xe lamp as a light source (100 mW cm^{-2}). The reactor cell consisted of three electrodes, a working electrode (fabricated film), a counter electrode (Pt wire), and a reference electrode (Ag/AgCl) in 0.1 M solution of Na_2SO_4 electrolyte. The electrochemical impedance spectroscopy (EIS) was also obtained by using the same electrodes and electrolyte solution. The hydrophilicity of films was measured by the contact angle system (POWER EACH, model JC2000DM), and the droplet images were taken through a CCD camera. The chemical state of TiO_2 film was measured via X-ray photoelectron spectroscopy (XPS).

Photodegradation Experiment

For solid-phase degradation, PS spheres solution (20 µL) was dropped on the catalyst films as well as on bare FTO (without catalyst) and dried at room temperature. Two UV lights (each UV light consists of four lamps with 32 W) were used as an artificial light source with a wavelength of 365 nm (3.05 mW cm^{-2}) and 254 nm (4.95 mW cm^{-2}) for the degradation of microplastics. 254 nm

UV light is deeper into the UV spectrum and typically generated about 90 % of the energy as compared to 365 nm. The photodegradation experiment was done in a lamp housing box (35 cm × 25 cm × 15 cm) under the ambient air condition, and the outside temperature was maintained by using a small air fan. The distance between the light source and the samples was 10 cm. All photodegradation experiments were carried out at room temperature without the addition of any oxidant, and each experiment was repeated three times, and average data is presented here.

The liquid phase degradation experiment was carried out by adding 0.05 g of TXT powder in 100 mL of PS solution (100 µL of PS (5 µm size) in 100 mL DI water). The solution was kept for stirring continuously during degradation reaction under 254 nm UV light irradiation, and samples were taken with the time interval.

Detection of Active Species

For the identification of relevant active species formed on the solid (microplastic)-solid (TiO_2) interface under UV light, different scavengers were added, e.g., ethylenediaminetetraacetic acid (EDTA) was used to scavenge the holes (h^+), tert-butyl alcohol (TBA) was used as a hydroxyl radical ($^{\bullet}OH$) scavenger, and the anaerobic experiment was conducted to check the role of oxygen. Briefly, the solutions of 10 mM EDTA and 1000 mM TBA were prepared in 2 mL of PS. 30 µL of PS solution with scavengers (EDTA and TBA) was dropped on TXT film for the detection of active species. Anaerobic hole scavenging experiment was conducted by placing the PS loaded TiO_2 film in an airtight reaction chamber (upper half part made of quartz and button half part made of Teflon, equipped with helical spin structure) under irradiation. Before irradiation, the air was removed from the chamber through the groove, and a vacuum environment was built through injection. The blank test was conducted without a photocatalyst (PS was dropped on cleaned FTO). All films were kept under UV light irradiation for 6 h, and analysis was done through SEM. The photodegradation of PS was observed to check the inhibition effect of these scavengers.

***In-situ* DRIFTS Experiment**

In-situ DRIFTS analysis was done on a Shimadzu FT-IR spectrometer (Tracer-100) armed with

a highly sensitive mercury cadmium telluride detector (MCTD) cooled through liquid nitrogen, and a temperature controller was fixed to the DRIFTS chamber to confirm the constant reaction temperature (Praying Mantis Kit, Harrick). For the *in-situ* DRIFT experiment, TiO_2 nanoparticles were prepared by the following method: TiO_2 precursor solution was dried for 6 h at 120 ℃ and then calcined at 450 ℃ with a ramping rate 5 ℃ min^{-1} for 30 min. The PS/TiO_2 composite was prepared by mixing 20 mL of PS solution (40 µL in 20 mL DI water) in prepared TiO_2 powder and dried at 70 ℃. A small proportion of PS/TiO_2 composite powder was used for DRIFTS experiment. The employed condition was: RH = 85 %, air (100 mL/min), and 365 nm UV light.

Intermediates Detection

The reaction intermediates during the PS degradation were detected by high-pressure photon ionization-time of flight mass spectrometry (HPPI-TOFMS) ion mass analyzer (Wang et al., 2016). The sample was prepared by dropping 40 µL solution of PS on TXT film which was dried at room temperature. For intermediates analysis, the prepared PS loaded TXT film was kept in a reaction chamber (upper half part made up of quartz and button part made up of Teflon, equipped with helical spin structure and the shallow groove) supplied with a continuous airflow under 365 nm UV light for 120 min. Employed relative humidity was 100 % at 25 ℃, and the HPPI-mass spectrum was recorded automatically.

End Product Analysis

Final products of microplastics degradation were analyzed by gas chromatography (SHIMADZU GC-2014). The concentration of end product was expressed in ppm. Sample for GC analysis was prepared by making the composite of 1 g of TiO_2 powder with 700 µL solution of PS and dried at 70 ℃. The obtained powder was put in a designed airtight quartz chamber under 365 nm UV light. Before reaction, the airtight chamber was vacuumed, and pure air was injected in it. Moreover, complete mineralization was examined through thermogravimetric analysis (TGA).

RAMAN Analysis of PE

The degradation of PE was investigated by using Raman xploRA plus spectrometer (HORIBA) following the RAMAN imaging technique, while the RAMAN spectrum was recorded with green laser (λ = 532 nm) as an excitation source. A visual search was done via Raman microscope objective 50x to take the image and spectrum of the selected area of PE with time intervals. Throughout the whole experiment, the same point was selected (all influencing parameters were kept the same) for the analysis of PE degradation

SUPPLEMENTAL REFERENCES

Ariza-Tarazona, M.C., Villarreal-Chiu, J.F., Barbieri, V., Siligardi, C., Cedillo-González, E.I., (2019). New strategy for microplastic degradation: Green photocatalysis using a protein-based porous N-TiO_2 semiconductor. Ceram. Int. 45(7), 9618-9624.

Ariza-Tarazona, M.C., Villarreal-Chiu, J.F., Hernandez-Lopez, J.M., Rivera De la Rosa, J., Barbieri, V., Siligardi, C., Cedillo-Gonzalez, E.I., (2020). Microplastic pollution reduction by a carbon and nitrogen-doped TiO_2: Effect of pH and temperature in the photocatalytic degradation process. J. Hazard. Mater. 395, 122632.

Decker, C., Mayo, F.R., (1973). Aging and degradation of polyolefins. II. γ-initiated oxidations of atactic polypropylene. Polymer Chem. Ed. 11(11), 2847–2877.

Kang, J., Zhou, L., Duan, X., Sun, H., Ao, Z., Wang, S., (2019). Degradation of Cosmetic Microplastics via Functionalized Carbon Nanosprings. Matter 1(3), 745-758.

Karthiga, R., Kavitha, B., Rajarajan, M., Suganthi, A., (2015). Photocatalytic and antimicrobial activity of $NiWO_4$ nanoparticles stabilized by the plant extract. Mater. Sci. Semicond. Process. 40, 123-129.

Satoh, N., Nakashima, T., Kamikura, K., Yamamoto, K., (2008). Quantum size effect in TiO_2 nanoparticles prepared by finely controlled metal assembly on dendrimer templates. Nat. Nanotechnol. 3, 106–111.

Shyichuk, A., White, J.J.J.o.A.P.S., (2000). Analysis of chain‐scission and crosslinking rates in the photo‐oxidation of polystyrene. J. Appl. Polym. Sci. 77(13), 3015-3023.

Tian, L., Chen, Q., Jiang, W., Wang, L., Xie, H., Kalogerakis, N., Ma, Y., Ji, R., (2019). A carbon-14 radiotracer-based study on the phototransformation of polystyrene nanoplastics in water versus in air. Environ. Sci. Nano 6(9), 2907-2917.

Wang, Y., Jiang, J., Hua, L., Hou, K., Xie, Y., Chen, P., Liu, W., Li, Q., Wang, S., Li, H., (2016). High-pressure photon ionization source for TOFMS and its application for online breath analysis. Anal. Chem. 88(18), 9047-9055.